Journal of The Electrochemical Society

Operando Synchrotron X-ray Diffraction Studies on TiS_2: The Effect of Propylene Carbonate on Reduction Mechanism

Journal of The Electrochemical Society, 2021 **168** 030514

Operando Synchrotron X-ray Diffraction Studies on TiS_2: The Effect of Propylene Carbonate on Reduction Mechanism

Raphaëlle G. Houdeville,[1] Ashley P. Black,[2] Alexandre Ponrouch,[2] M. Rosa Palacín,[2] and François Fauth[1,z]

[1]*CELLS-ALBA Synchrotron, Cerdanyola del Valles, Barcelona, Spain*
[2]*Institut de Ciència de Materials de Barcelona, ICMAB-CSIC, Campus UAB, 08193 Bellaterra, Catalonia, Spain*

We present herein a systematic study of solvent co-intercalation during electrochemical reduction of titanium disulfide in lithium cells using state of the art *in situ* cells and synchrotron X-ray diffraction. To understand the role of the electrolyte components, four salts ($LiBF_4$, LiBOB, $LiPF_6$ and LiTFSI) and three solvents (ethylene carbonate, propylene carbonate and dimethyl carbonate) were investigated. Various types of *in situ* cells were assembled and X-ray diffraction patterns were collected in *operando* upon cycling. Co-intercalated phase formation was found to be triggered by the presence of propylene carbonate and to be electrochemically driven. This co-intercalated phase is formed in the early stages of reduction, with cell parameters a = 3.514 Å, c = 17.931 Å, corresponding approximately to a tripling of the pristine TiS_2 cell along the c-axis. This phase does not seem to evolve upon further oxidation and hence induces an overall loss of capacity. Whereas the nature of the anion does not appear to influence the co-intercalated phase formation, the content of propylene carbonate in the electrolyte is clearly correlated to both its amount and the extent of capacity loss.

 [DOI: 10.1149/1945-7111/abe983]

Manuscript submitted December 16, 2020; revised manuscript received February 2, 2021. Published March 8, 2021.

Supplementary material for this article is available online

Intercalation chemistry has been a cornerstone in the development of Li-ion batteries as a commercial product, with layered sulfides being amongst most investigated class of compounds as potential positive electrodes.[1]

Moreover, TiS_2 coupled to first lithium metal,[2] and then a lithium aluminium alloy, enabled building of successful cell prototypes at Exxon in the late 70's and 80's by Stan Whittingham's team, including both larger cells (45 Wh)[3] and smaller (25 mAh or 100 mAh) prototypes, the latter still keeping > 50% of its initial capacity after 35 years.[4]

Despite sulfides being soon practically superseded by oxides to almost double voltage at cell level, TiS_2 has continuously been a paradigm within intercalation compounds and also became a benchmark material to assess multivalent intercalation chemistry.[5–7]

In situ and *operando* diffraction studies on batteries were very early identified as a precious tool to get a mechanistic understanding of the lithium ion intercalation in TiS_2.[8,9] Indeed, they avoid the drawbacks imposed by *ex situ* studies related to the preparation of samples in different redox stages, which also involves some risk of the electroactive phase being altered (evolution of metastable phases, contamination by air or humidity, etc.) during handling. Moreover, *operando* experiments enable an extension of studies to grasp the influence of the testing protocol (rate, temperature, etc.). While not possible in the early days of Li-ion battery developments, the use of synchrotron radiation considerably increases data collection statistics and improves time and angular resolution, even when compared to the latest generation of laboratory diffractometers.[10]

The early studies aimed at elucidating the redox mechanism of TiS_2 from a structural point of view (typically single phase vs two phase). Despite data not enabling complete structural refinement, confrontation with results of chemical intercalation using lithium solutions in ammonia[11,12] or solutions of n-butyl lithium in hexane,[13] were very useful to fully understand the nature and structure of the phases formed. In particular, the work of Thompson and co-workers to prepare and analyze Li_xTiS_2 with different x values from 0 to 1 mol serves as a good support for comparison.[13] The first *operando* study was performed by Chianelli et al.[5] and allowed to assess that the insertion mechanism was single phase with formation of a solid solution and, using complementary techniques, information on nucleation and diffusion was gathered throughout the cycle. Later on, Dahn and co-workers reinvestigated this mechanism with a different cell design.[9] The electrolyte used was at that time seldom considered as an essential parameter affecting the nature of the Li insertion process. Chianelli et al. used 2 M $LiClO_4$ in dioxolane whereas Dahn and co-workers used 1 M $LiAsF_6$ in propylene carbonate (PC) and mentioned co-intercalation of PC at high voltages, despite being deemed to be a minor feature and not further investigated. With respect to electrochemical conditions, Chianelli et al. operated in standard galvanostatic mode (ca. C/16 to C/32), while Dahn et al. used similar rates but a much slower pulsed protocol enabling equilibration of electrode, which was assessed by comparing two patterns taken in open circuit with 10 h difference.

In this paper, we present further *operando* studies on the intercalation of lithium in TiS_2 using synchrotron radiation with the aim of shedding further light on the influence of the electrochemical protocol and electrolyte used in the phases formed. In particular, $LiPF_6$, $LiBF_4$, lithium bis(trifluoromethanesulfonyl)imide (LiTFSI) and lithium bis-oxalatoborate (LiBOB) salts in different alkylcarbonates (including PC) were investigated. This study unveiled some features related to the co-intercalation and correlations with electrochemistry, enabling to get a more comprehensive picture of the process.

Experimental

The working electrodes consisted of a powder mixture of TiS_2 from Sigma-Aldrich (purity 99.995%), carbon black (Super P, Timcal) and polyvinylidene fluoride (PVDF) from Sigma-Aldrich (Mw ~ 534,000 g mol^{-1}) in weight ratios of 84:10:6 prepared by manual grinding with mortar and pestle. The powders were manipulated and stored in an argon filled glovebox (<0.5 ppm of O_2, < 0.5 ppm H_2O). In an attempt to decrease the impact of preferred orientation, loose powder is used directly as a cathode. For each *in situ* data collection on *operando* conditions, a capillary of the electrode material was collected prior to the experiment. These data were used for alignment purposes as well as to ensure the pristine material was not altered. Because of the preferred orientation issues,

[z]E-mail: ffauth@cells.es

in situ data in *operando* were refined by the LeBail[14] method to extract the unit cell parameters which are satisfactory indicators of the lithium insertion in TiS_2. Indeed, the low scattering strength of Li prevents extracting reliable Li site occupation by Rietveld refinement.

LP30 electrolyte from Sigma-Aldrich (1 M $LiPF_6$ in ethylene carbonate (EC):dimethyl carbonate (DMC) 1:1 (v:v), battery grade) was used. A 0.67 M $LiPF_6$ in EC:DMC:PC solution at a volumetric ratio of 33:33:33 (v:v:v) was also prepared by adding PC (Aldrich anhydrous 99.7%) to the commercial LP30. 1 M LiTFSI (Sigma-Aldrich, ⩾ 99%), 1 M LiBOB (Chemetall, 99.99%) or 1 M $LiBF_4$ (Alfa Aesar, 99.97%) were prepared using a 1:1(v:v) mixture of EC (Aldrich anhydrous 99.0%) and PC as solvent. For the PC concentration study in addition to some of the above mentioned, 1 M $LiPF_6$ (Alfa Aesar, 98%) dissolved in a 1:1 mixture of EC and DMC (Sigma Aldrich, anhydrous, ⩾99%), as well as in a 2:1:2 (v:v:v), mixture of EC:DMC:PC, 3:2 (v:v) of EC:PC, 3:7 (v:v) of EC:PC or in pure PC were prepared. Handling and electrolyte preparations were conducted in an argon filled glovebox.

Electrochemistry was monitored using a Bio-Logic VSP potentiostat. Prior to cycling, cells were kept at open circuit voltage (OCV) for periods ranging from 1 to 5 h. The cycling protocol consisted of Galvanostatic cycling with Potential Limitation (GCPL) at either C/5 or C/15, i.e. inserting 1 mol of Li per mol of TiS_2 in 5 or 15 h, respectively. To assess the phase stability at the end of each oxidation or reduction cycle, the potential was fixed for 1 h and several patterns were collected. The cutoff voltages were set at 1.5 V and 3 V vs Li^+/Li to allow the complete Li (de-)insertion. However, in the case of LiBOB, the cutoff voltage was lower (1.8 V vs Li^+/Li) in order to avoid the anion reduction close to this value as reported in Panitz et al. work.[15] This prevented the complete Li insertion as was demonstrated by collecting data in the same voltage window with $LiBF_4$ in EC:PC. The *operando* measurements were conducted at ALBA synchrotron on the powder diffraction station of the BL04-MSPD beamline,[16,17] using the position sensitive detector MYTHEN at 15 keV (λ = 0.826 Å) beam energy. The exact wavelength was determined for each experimental session from Bragg reflections of silicon SRM640d NIST standard. The XRD patterns were collected in the $\approx 2.3 \leqslant 2\theta \leqslant 48°$ range, with 72 s effective integration time, ensuring 10 min frequency between successive patterns. Pristine electrode material was measured in a spinning 0.7 mm capillary to get better statistics. Cells were centered on the diffractometer by comparing the patterns with previously measured TiS_2 in capillary. This alignment procedure consisted in adjusting the position of the cell along the incoming beam. The lattice parameters were extracted from the patterns using the LeBail refinement method as implemented in the FullProf suite software.[14] In the case of the pristine material capillary, full structure Rietveld refinement was applied.

Operando electrochemical tests were performed using two types of *in situ* cells: Swagelok-type cells described by J.B. Leriche et al.[18] and drilled coin cells with glass window as used by Herklotz.[19] Lithium disks of 16 mm of diameter and 0.6 mm thick from MTI Corporation (Richmond, CA, USA) were used as counter electrodes. One glass fiber filter disk (Whatman, GE Healthcare, 420 μ thick) was used as separator. An aluminum foil (0.010 mm, 99%, GoodFellow) was placed on the cathode side to protect the beryllium or glass window and ensure good electric contact. Both types of cell were mounted on the powder diffraction instrument using a tailor-made sample holder made at ALBA that enables an automatized sequential measurement of 3 and 4 cells in case of the Leriche and coin cell setup, respectively. For each of the *in situ* cells, data were collected during the OCV up to 5 h to detect any spontaneous evolution related to immersion in the electrolyte (shortcut or spontaneous reaction).

A series of complementary electrochemical tests were performed out of the beam in three electrode Swagelok cells.[20] Metallic lithium disks were used as counter electrodes and the reference electrode consisted in a piece of lithium, supported by a copper grid and attached to a tailored plunger as described by Dugas et al.[21] TiS_2 tape electrodes were prepared as described by Verrelli et al.[7] Cells were kept at OCV for 2 h and cycled between 1.5 V and 2.85 V at C/15.

Results and Discussion

Characterization of pristine sample.—Titanium disulfide crystalizes in the hexagonal system, space group $P\bar{3}m1$. Its structure is characterized by the presence of titanium atoms within sulfur octahedra which are sharing edges and form layers exhibiting a hexagonal stacking along the *c*-axis. Because of this lamellar structure, preferred orientation was expected for patterns corresponding to *in situ* cells but surprisingly occurred as well for samples sealed inside capillaries. Figure 1 depicts the patterns and refinement corresponding to the electrode powder mix measured in a rotating capillary a) and a pattern collected in a coin-cell after its assembly b). In that case, the electrolyte used was LP30. All parasitic peaks, related to the aluminum current collectors or lithium foil, were excluded from the refinement. The patterns exhibit significant differences in the relative intensities of the 001 and 110 peaks. The 001 peak is the second most intense peak in the pattern corresponding to the capillary while its intensity is decreased by

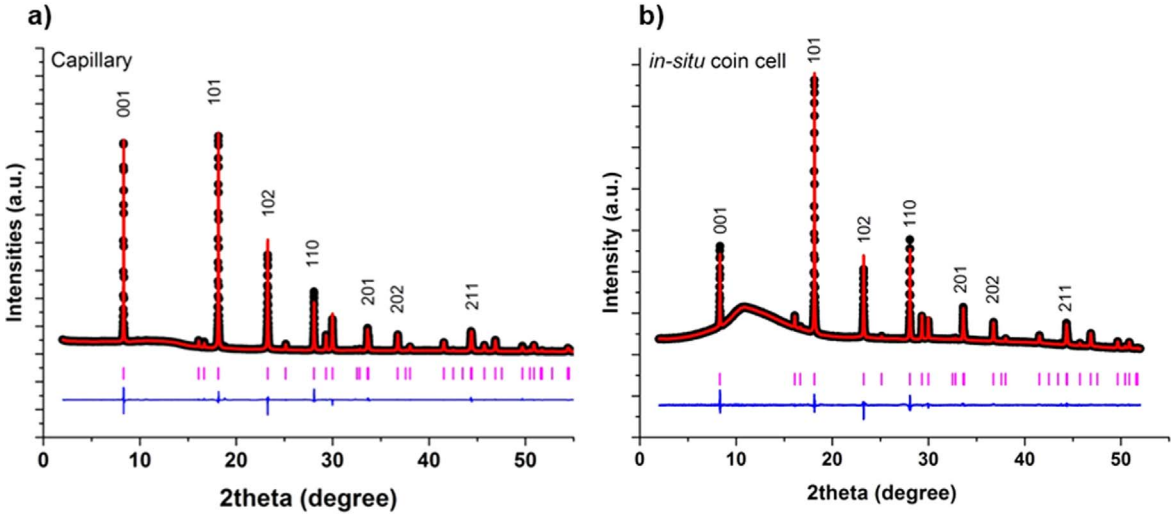

Figure 1. Observed and calculated synchrotron X-ray powder diffraction patterns for TiS_2 electrodes measured in capillary (a) and in an in situ cell assembled with LP30 (b).

about half in the pattern corresponding to the cell. The peak ratio is also different when focusing on the 102 and 110 reflections. In the capillary, the 102 peak is more intense than the 110 while it is the opposite in the *in situ* cell. Patterns were refined using the Rietveld method taking the structure reported by Bear and McTaggart (ICSD card N° 651178).[22] For preferred orientation correction, the March function as implemented in the Fullprof suite was applied assuming orientation along the *Z*-axis. For the pattern corresponding to the capillary, the parameter translating the preferred orientation was found to be Pref1 = 0.749 while for the one corresponding to the *in situ* cells, in that case a coin cell, Pref1 = 1.379. The strong preferred orientation associated to the platelet-like TiS_2 crystallites was not totally suppressed by rotating the capillary. Indeed, the strong intensities measured on the 00l reflections indicate that the crystallites were stacked horizontally inside the 0.7 mm capillary, exposing the 00l planes parallel to diffraction plane and therefore over estimating the 00l reflections in transmission geometry. The same horizontal stacking of platelet-like crystallites takes place in the *in situ* cells but these are now allocated perpendicular to the beam minimizing the 00l and increasing the hk0 reflections collected at the detector in a transmission mode. Furthermore, when measuring a tape-casted electrodein an *in situ* cell, the preferred orientation was so critical that the reflection along the 00l plane were suppressed from the patterns.

Another feature clearly visible on both patterns resides in the background increase at angles lower than $2\theta \leqslant 20°$ in the pattern corresponding to the capillary and a bump centered at $2\theta \sim 12°$ in the one corresponding to *in situ* cells (see Figs. 1a and 1b respectively). The former effect arises from the amorphous carbon exhibiting scattering in the small angle regime.[23] The bump in background occurs only for cells already loaded with the electrolyte, and its intensity is higher than the carbon contribution. This background bump position is solvent dependent centered at 3.9 Å d-spacing for LP30 and gradually moving towards higher d-spacing when increasing the PC content, reaching 4.3 Å when the electrolyte only contains PC as a solvent, as depicted in Fig. S1. This may be related to the position of the solvent molecule in the solvation shell of the ion in the electrolyte.

Operando *experiments.*—*In situ* cells were prepared and tested as described in the experimental section, starting upon reduction and collecting patterns every 10 min. All data collection begins by, at least, a 1 h at OCV and no spontaneous reaction was observed. These patterns were refined to find a lattice where $a = 3.409$ Å and $c = 5.700$ Å which are in good accordance with data already reported in the literature.[22] Figures 2a, 2c and 2e display the characteristic galvanostatic profiles of TiS_2 electrodes subjected to 1 h OCV followed by GCPL tests at C/15 in coin cells. The electrolytes used were LP30, $LiPF_6$ in EC:DMC:PC (2:1:2) and LiTFSI in EC:PC (1:1), respectively. The corresponding *operando* XRD patterns collected with the routine described above are shown in Figs. 2b, 2d, and 2f. On the X-ray diffraction patterns b and f, the beam was lost for a short period, causing the loss of 5 patterns at the end of the reduction (from pattern 91 to 95 incl.).

The patterns corresponding to the cell cycled with LP30 are consistent with the typical lithium insertion process expected in TiS_2. During the reduction, the Li_xTiS_2 solid solution starts to form, as well documented previously[8,9,24] and pristine TiS_2 reflections shifting towards lower angles which indicate that the lattice is expanding, first along the *c-axis*, and later along the *a*- and *b-axis*. At the end of the reduction the lattice parameters were refined to find $a = 3.458$ Å and $c = 6.187$ Å, in good accordance with values reported in literature for the $LiTiS_2$ phase.[8,13,25] Upon re-oxidation, the reverse process takes place. A second reduction step was carried out to evaluate the reversibility of the process.

To assess the coherence of our data, a comparison was made with the data published by Thompson[13] derived from blending TiS_2 and $LiTiS_2$ powders in different proportions and annealing them to achieve Li_xTiS_2 with different values of x. Figure 3a presents the lattice parameters *a* and *c* corresponding to Li_xTiS_2 at different lithium contents obtained from LeBail refinement of synchrotron diffraction data collected while cycling in two different PC-free electrolytes, in comparison with the values obtained by Thompson. While Thompson's data is presented with respect to the x calculated following the mixtures prepared, our data was plotted directly using the x value deduced from the electrochemical experiments considering that lithium intercalation is the only redox process taking place. The comparison was made for two experiments done with different electrolytes: LP30 cycled at C/5, and 1 M LiTFSI in EC:DMC (1:1)(v:v), cycled at C/15. In the early stages of reduction ($0 \leqslant x \leqslant 0.35$ mol), the *c*-parameter increases rapidly with a sharp slope while the *a*-parameter grows moderately. Above $x > 0.35$ mol, the *c*-parameter saturates at 6.19 Å while the slope of the *a*-parameter increases progressively until reaching 3.458 Å for one inserted lithium.[13]

In the case of PC-containing electrolytes (Figs. 2d, 2f and S3b) the X-ray diffraction patterns exhibit intense peaks at $2\theta \approx 2.7°$, 5.4° and 8.1° appearing at the very early stage of reduction together with the peaks corresponding to Li_xTiS_2. These values correspond to significantly large real space d-spacing (17.52, 8.76 and 5.85 Å at the end of the reduction, respectively for the 3 first reflections), which is approximately three times larger than the pristine lattice along the *c*-axis. Some low angle peaks with similar d-spacing were also mentioned by Dahn and coworkers (17.8 Å) and Whittingham (18.4 Å)[9,24] and related to propylene carbonate co-intercalation but not further investigated. This new phase exhibiting an expanded *c*-parameter will later be mentioned as co-intercalated phase. To study in depth this phenomenon a series of *operando* experiments with different salts and PC containing solvents have been conducted.

Concomitant to the formation of the co-intercalated phase, the intensity of the Bragg reflections of the TiS_2 phase drops by 70%–80% as depicted in Fig. S2. Interestingly, in the early stages of lithium insertion, while the reflections of the Li_xTiS_2 phase drift towards lower angles, the reflections of the co-intercalated phase shift toward higher angles, indicating a contraction of the lattice from 17.96 Å to 17.52 Å in average (from $2\theta = 2.63°$ to 2.70°). Though no explanation was found, this phenomenon is reproducible. Upon reoxidation, the cell parameters of Li_xTiS_2 phase decrease as lithium is deinserted, but the peaks corresponding to the co-intercalated phase remain unchanged, which was already documented by Dahn.[9] However, this phenomenon is not reversible in all systems as described by Tchitchekova et al.[6] and Verrelli et al.[7] Tchitchekova et al. were using $Ca(BF_4)_2$ 0.45 M in EC:PC at 100 °C and Verrelli et al. were using either $Ca(BF_4)_2$ or $Ca(TFSI)_2$ 0.3 M in PC, at either room temperature, 60 °C or 100 °C. In all these cases, a phase similar to ours was observed, with larger cell parameters, which disappears upon reoxidation, indicating a reversibility of co-intercalation in those cases. We tentatively ascribed this difference of reversibility for the co-intercalated phases in Li and Ca cells to the fact that Li and Ca cation complexes present different coulombic interactions with the host structure. Note also that Tchitchekova et al.[6] mentioned a co-intercalated phase appearing upon reduction with $Mg(TFSI)_2$ 0.3 M in EC:PC but no re-oxidation was reported on that paper, therefore we cannot conclude on the reversibility of the co-intercalation in this system. Though the co-intercalation is irreversible with lithium, it is still possible to perform further reduction/oxidation cycles, with the only changes observed being related to the Li_xTiS_2 phase, as proven by the second reduction performed on these two cells. Other experiments carried out using both types of *in situ* cells, faster C-rates, other solvent mixtures and salts are coherent with the data presented (see Figs. S3 and S4).

The *a* and *c* parameters of the Li_xTiS_2 phase as function of the lithium inserted using LP30 and 1 M $LiPF_6$ in PC at C/5 rate are shown in Fig. 3b, The results are compared with those reported by Dahn and co-workers in an *in situ* cell using 1 M $LiAsF_6$ in PC as electrolyte.[9] Although Dahn's and Thompson's[13] curves are similar, we observe a discrepancy with our data at early stages of reduction ($0 \leqslant x \leqslant 0.28$) resulting in a smaller hysteresis. Knowing from

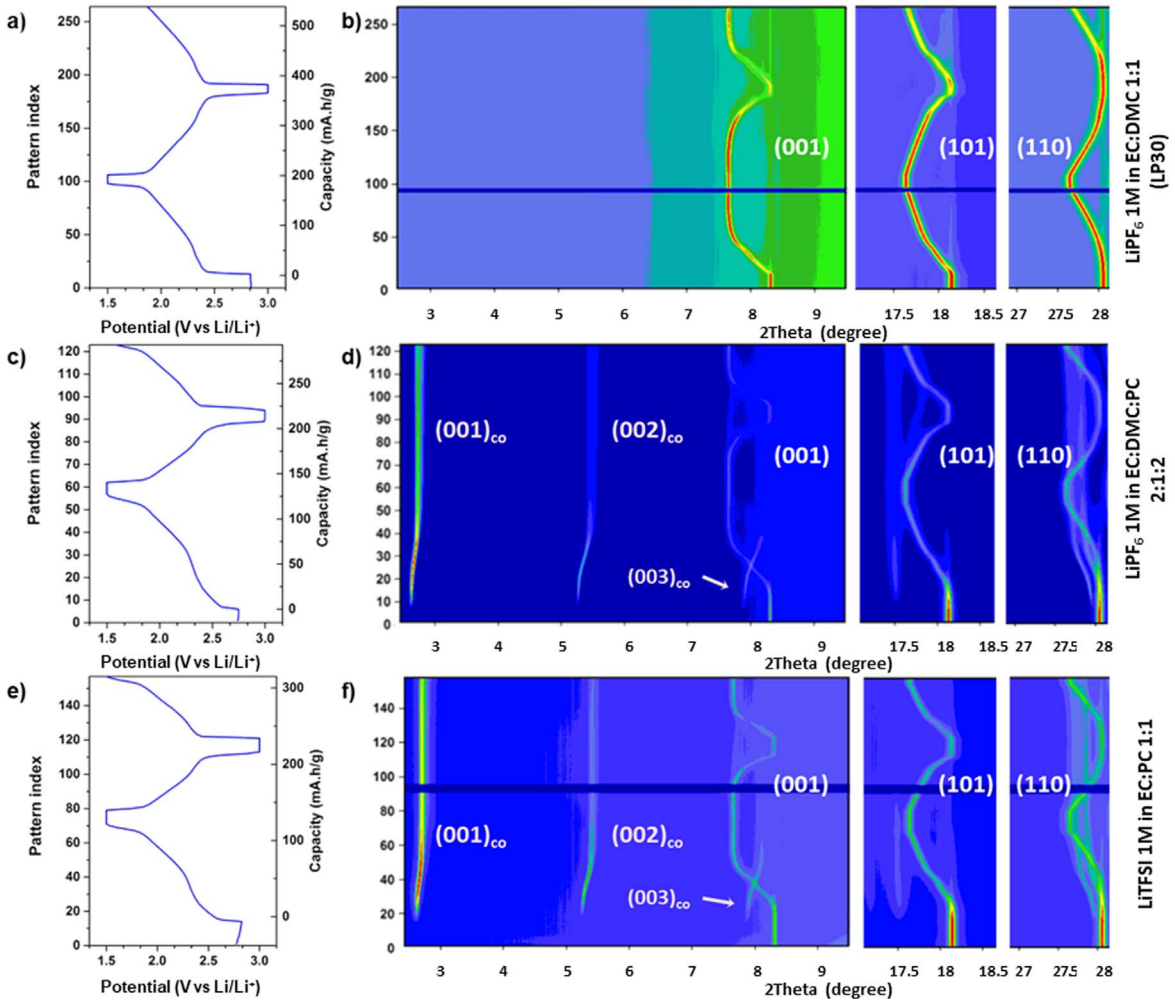

Figure 2. Pattern number (10 min increment in time) vs voltage and associated X-ray surface plots of cells cycled with (a)–(b) LP30, (c)–(d) $LiPF_6$ 1 M in EC:DMC:PC 2:1:2 and (e)–(f) LiTFSI 1 M in EC:PC 1:1.

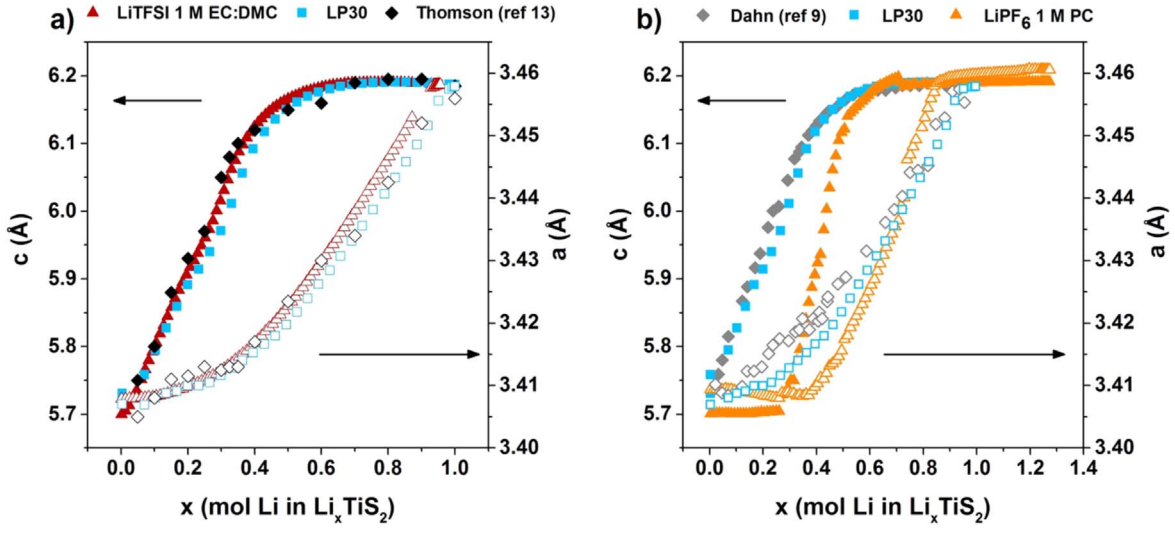

Figure 3. Comparison of the Li_xTiS_2 phase lattice parameters upon reduction for experiments carried out with different electrolytes. Full symbols represent the *c*-axis parameter (left), empty symbol the *a*-axis (right). (a) Black diamonds are the data retrieved from Ref. 13, blue squares correspond to data resulting from the experiment carried out with LP30 electrolyte at C/5 and red triangles to those derived from 1 M LiTFSI in EC:DMC (1:1) at C/15. (b) Grey diamonds represent data taken from Ref. 9, blue squares correspond to data resulting from the experiment carried out with LP30, and orange triangles to 1 M $LiPF_6$ in PC.

Figs. 2d, 2f that PC is co-intercalated at early stage of reduction, the range $0 \leqslant x \leqslant 0.28$ shown in Fig. 3b does not correspond to the real amount of lithium in Li_xTiS_2. A method to calculate the experimental capacity related to the formation of Li_xTiS_2 will be developed later in this article.

In order to get further insights into the structure evolution of the co-intercalated phase trough the reduction process a LeBail refinement was carried out for the XRD patterns corresponding to early stages and at the end of the first reduction of TiS_2 electrodes cycled in 1 M $LiPF_6$ in EC:DMC:PC 2:1:2 electrolyte shown in Fig. 2b, pattern 15 and 60, respectively. The results are displayed in Fig. S5. The patterns were refined considering two phases, the Li_xTiS_2 that follows lattice parameter evolution related to the formation of the solid solution through the reduction process and a co-intercalated phase that appears at early stages of reduction characterized by its low angle reflections at $2\theta \approx 2.7°$, 5.4° and 8.1°. Both phases were fitted in the hexagonal space group $P\bar{3}m1$. In Fig. S5a, in addition to these two phases, aluminum and lithium from the current collector and counter electrode, respectively, were considered in the fitting while for Fig. S5b they were considered as excluded regions for aim of clarity. The lattice parameters of the co-intercalated phase were found to be $a = 3.514$ Å and $c = 17.931$ Å at early stages of reduction (pattern15) and $a = 3.5835$ Å and $c = 17.155$ Å at the end of first reduction (pattern 60). Attempts to probe the configuration of the co-intercalated PC molecule by IR were hindered by the low resolution of the spectra in the carbonyl stretching region.[26]

To assess the independence of the co-intercalation from the salt and to make sure the presence of PC in the electrolyte is the only key factor triggering the co-intercalation process, reduction was performed using the four salts tested in a solvent mix that contained PC, using the same configuration and program as before, except for the cell containing $LiBF_4$ where a Leriche cell was used instead of a coin cell. The electrolytes tested were 1 M of either LiBOB (i), $LiBF_4$ (ii) or LiTFSI (iv) in EC:PC (1:1) and PC added to LP30 resulting in a 0.67 M $LiPF_6$ in EC:DMC:PC (33:33:33) electrolyte (iii). The voltage vs capacity plots for the first reduction are presented in Fig. 4a. Patterns have been collected *operando* through the whole reduction and reoxidation, (see figure S3) but only the last pattern of the reduction is presented in Fig. 4b to compare eventual structural changes. The reduction curves are similar with no significant impact of the salt. A little bump is visible at low capacity around 2.5 V on the reduction curve of the cell containing LiBOB, but this feature is not salt dependent and will be discussed later. Regarding the diffraction pattern, in addition to the Li_xTiS_2 reflections, new peaks can be observed, principally at low angles ($2\theta \approx 2.7°$, 5.4° and 8.1°) as seen in Fig. 2. Patterns were normalized with respect to the $LiTiS_2$ 001 reflection (7.64°). Peak intensities are comparable in all cases, indicating that the nature of the anions present in the electrolyte does not have a significant influence in the formation the co-intercalated phase. Patterns corresponding to reduction of TiS_2 in cells using the same electrolyte salts but either EC or EC:DMC (1:1) as solvents do not show any co-intercalation peaks, indicating that these are triggered by the presence of PC.

Figure 5a depicts synchrotron X-ray diffraction patterns of titanium disulfide electrodes at the end of reduction for cells cycled with $LiPF_6$-based electrolytes but different PC content. The electrolytes tested were 1 M $LiPF_6$ in EC:DMC (1:1), 0.67 M $LiPF_6$ in EC:DMC:PC (33:33:33), 1 M $LiPF_6$ in EC:DMC:PC (2:1:2), 1 M $LiPF_6$ in EC:PC 2:3, 1 M $LiPF_6$ in EC:PC 3:7 and 1 M $LiPF_6$ in PC. Patterns were normalized with respect to the $LiTiS_2$ 001 reflection (7.64°). The electrochemical curves and the X-ray diffraction data collected throughout the full experiment (two cycles) are presented in Fig. S4. A pseudo plateau is visible on the cell cycled with the electrolyte containing 100% PC (Fig. S3g) at ca. 1.55 V after inserting ≈0.8 mol of lithium. In all electrolytes, the reflections of both Li_xTiS_2 and co-intercalated phases are found at the same position, meaning that the cell parameters of the co-intercalated phase are not dependent on the electrolyte composition. However, the intensity of the peaks related to the co-intercalated phase increases with the PC content, while the intensity of the peaks related to Li_xTiS_2 phase decrease. In an attempt to quantify the amount of co-intercalated phase formed, the ratio between the intensity of the 001 peak of the co-intercalated phase at the end of the reduction and the 001 peak of the pristine TiS_2 was calculated for each electrolyte. The resulting values are plotted as a function of the PC content in the electrolyte in Fig. 5b. As the amount of PC in the electrolyte increases, the ratio between the two phases increases, confirming the observation that more co-intercalated phase is formed, the maximum of intensity being observed with the $LiPF_6$ in 100% PC electrolyte. The surface plots of the data collected throughout the cycling for 0%, 33%, 40% and 100% of PC are available in Fig. S3.

In an attempt to link the capacity loss with the crystallography, Fig. 6a was built similarly to Fig. 3. Figures 6a and 6b present the lattice parameters a and c of Li_xTiS_2 at different lithium contents obtained from LeBail refinement of synchrotron *operando* diffraction data collected in either LP30 or 0.67 M $LiPF_6$ in EC:DMC:PC (33:33:33), in comparison with the data from.[9] The corresponding electrochemical curves are presented in Fig. S5. In this case, the plot seems to be compressed along the x-axis, the data not matching Dahn's trend. Indeed, the x is calculated considering that the only electrochemical process taking place is lithium insertion into TiS_2 to form Li_xTiS_2, without taking into account the charge related to formation of the co-intercalated phase. Thompson[13] described three

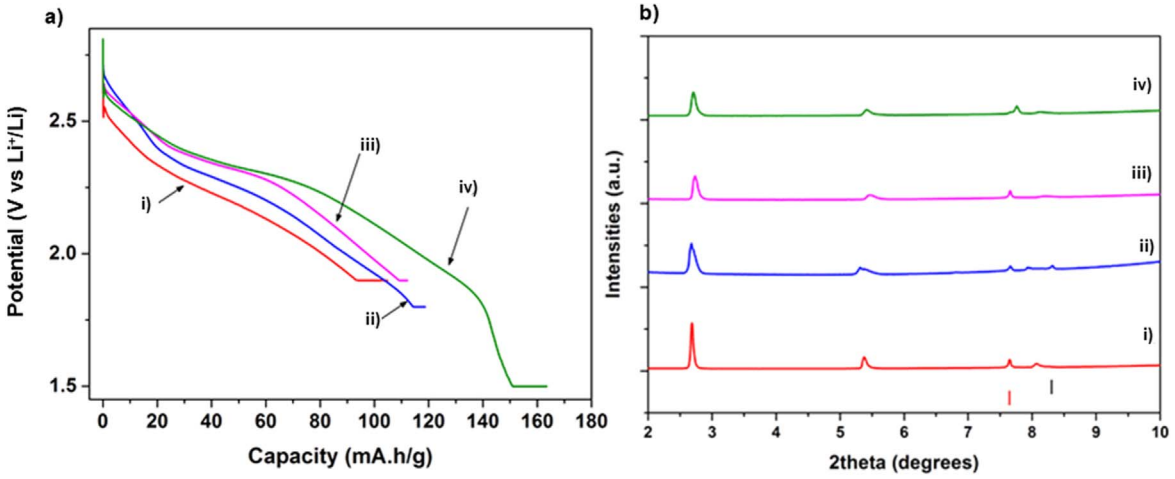

Figure 4. Electrochemical reduction curve (a) and last reduction SXRD patterns (b) of cells cycled with (i) 1 M LiBOB in EC:PC (1:1), (ii) 1 M $LiBF_4$ inEC:PC (1:1), (iii) 0.67 M $LiPF_6$ in EC:DMC:PC (33:33:33) and (iv) 1 M LiTFSI in EC:PC (1:1). Black and red ticks represent the 001 reflection of pristine TiS_2 and $LiTiS_2$ respectively.

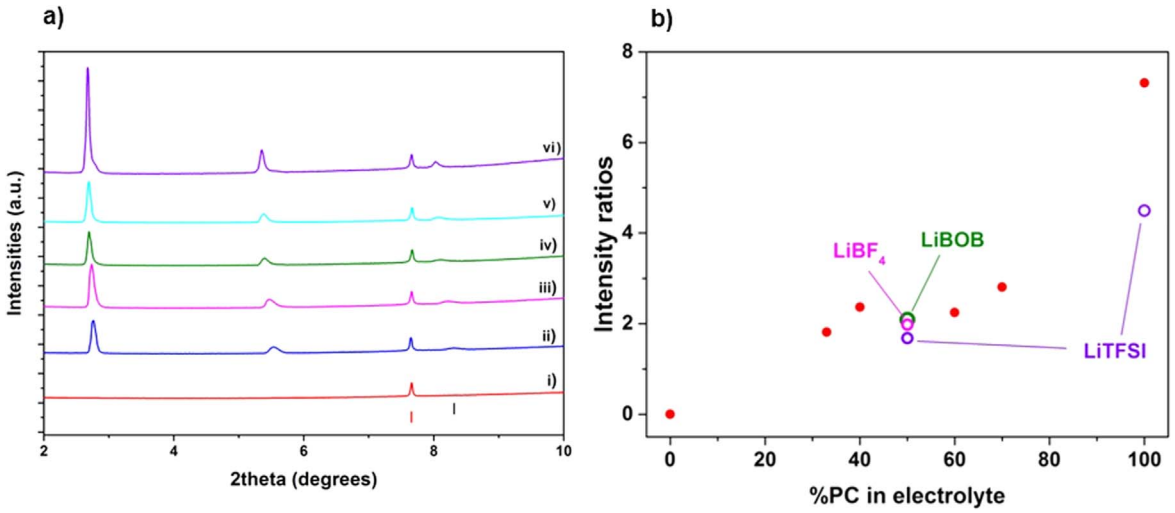

Figure 5. (a) Last reduction SXRD pattern of cells cycled with $LiPF_6$ based electrolytes, (i) 1 M in EC:DMC (1:1), (ii) 0.67 M in EC:PC:DMC(3:3:3), (iii) 1 M In EC:PC:DMC (2:2:1), (iv) 1 M in EC:PC 2:3, (v) 1 M in EC:PC 3:7 and (vi) 1 M in PC. Black and red ticks represent the 001 reflection of pristine TiS2 and LiTiS2, respectively; (ii) intensity ratio between the 001 co-intercalation peak and 001 pristine TiS_2 peak as a function of the proportion of PC in the electrolyte. Red dots correspond to $LiPF_6$-based electrolytes, pink circle to $LiBF_4$, green circle to LiBOB and purple circles to LiTFSI.

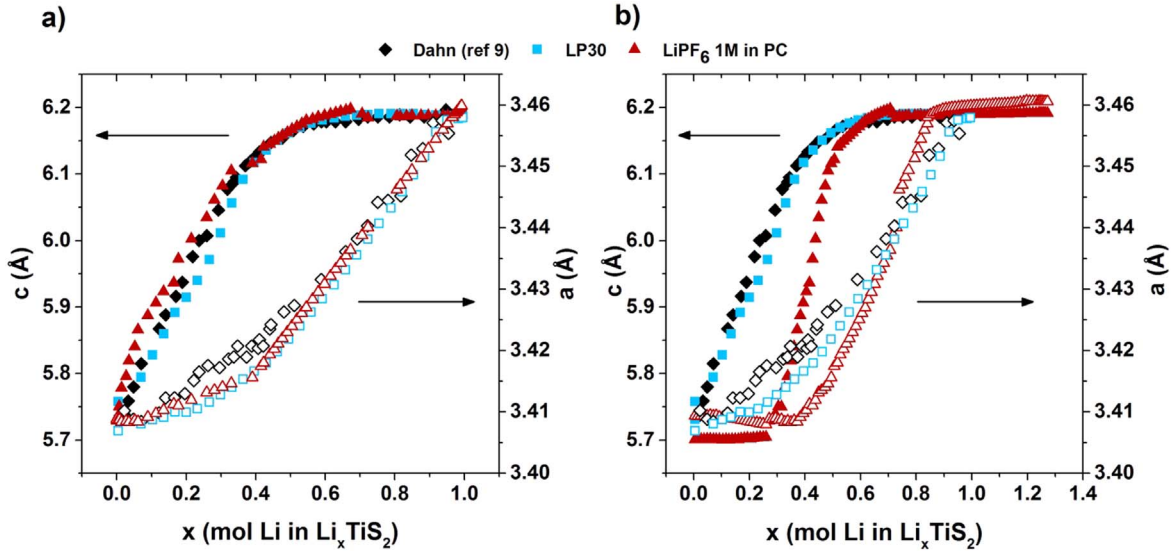

Figure 6. Comparison of the $LixTiS_2$ phase lattice parameters upon reduction of TiS_2 in several cells using different electrolytes. Left plot depicts the data without correction, right plot depicts the same points but where x is corrected using the method described. Full symbols represent the values along the *c*-axis (left), empty symbol along the *a*-axis (right). Diamonds are the data retrieved from Ref. 5, blue squares were obtained from the experiment using LP30 electrolyte and red triangles with 0.67 M $LiPF_6$ in EC:PC:DMC (33:33:33).

pseudo-linear zones of the curves: between x = 0 mol and x = 0.35 mol for both *a* and *c* parameter, and between x = 0.35 mol and x = 1 mol for the a-parameter only. Linear regression was applied to these zones on the curve corresponding to LP30 to obtain formulas linking the lattice parameters and x. Thanks to these formulas the x was recalculated and fits better the curve from Dahn and LP30, which is representative of the amount of lithium inserted. This confirms that the formation of the co-intercalated phase does not affect the formation of Li_xTiS_2. Moreover, as seen in Fig. 2, the co-intercalation is irreversible. This seems to indicate that the TiS_2 particles that reacted to form the co-intercalated phase are unable to de-intercalate lithium afterwards, creating an electrochemically dead mass with respect to the Li intercalation which is coherent with the reversible capacity loss observed (see Fig. S6).

To point out how the co-intercalation affects the reversible capacity, a series of tests was carried out *ex situ* in three-electrodes Swagelok cells using a TiS_2 tape electrode. Electrolytes tested were 1 M $LiPF_6$ in either EC:DMC (1:1), EC:DMC:PC (33:33:33), EC:DMC:PC (2:1:2), EC:PC (3:7) or PC. Electrochemical curves for the first reduction are presented in Fig. 7a while the capacity at the end of the reduction and the reversibility of the first cycle are plotted vs the amount of PC in Figs. 7c and 7d, respectively. The reversibility is the ratio between the reoxidation capacity and the reduction capacity. It appears clearly that the more the electrolyte contains PC, the more the capacity and the reversibility of the first cycle are decreasing. Here again, it seems that the capacity and reversibility loss are proportional to the amount of PC in the electrolyte, which implies that the capacity loss may be linked to the amount of co-intercalated phase formed.

Another interesting electrochemical feature, solely observed for PC containing electrolytes, appears at the beginning of the first reduction (at ca. 2.5 V and can be appreciated in Fig. 7b). After the initial potential drop, the voltage re-increases before decreasing again, creating some bump in the curve. The more the electrolyte

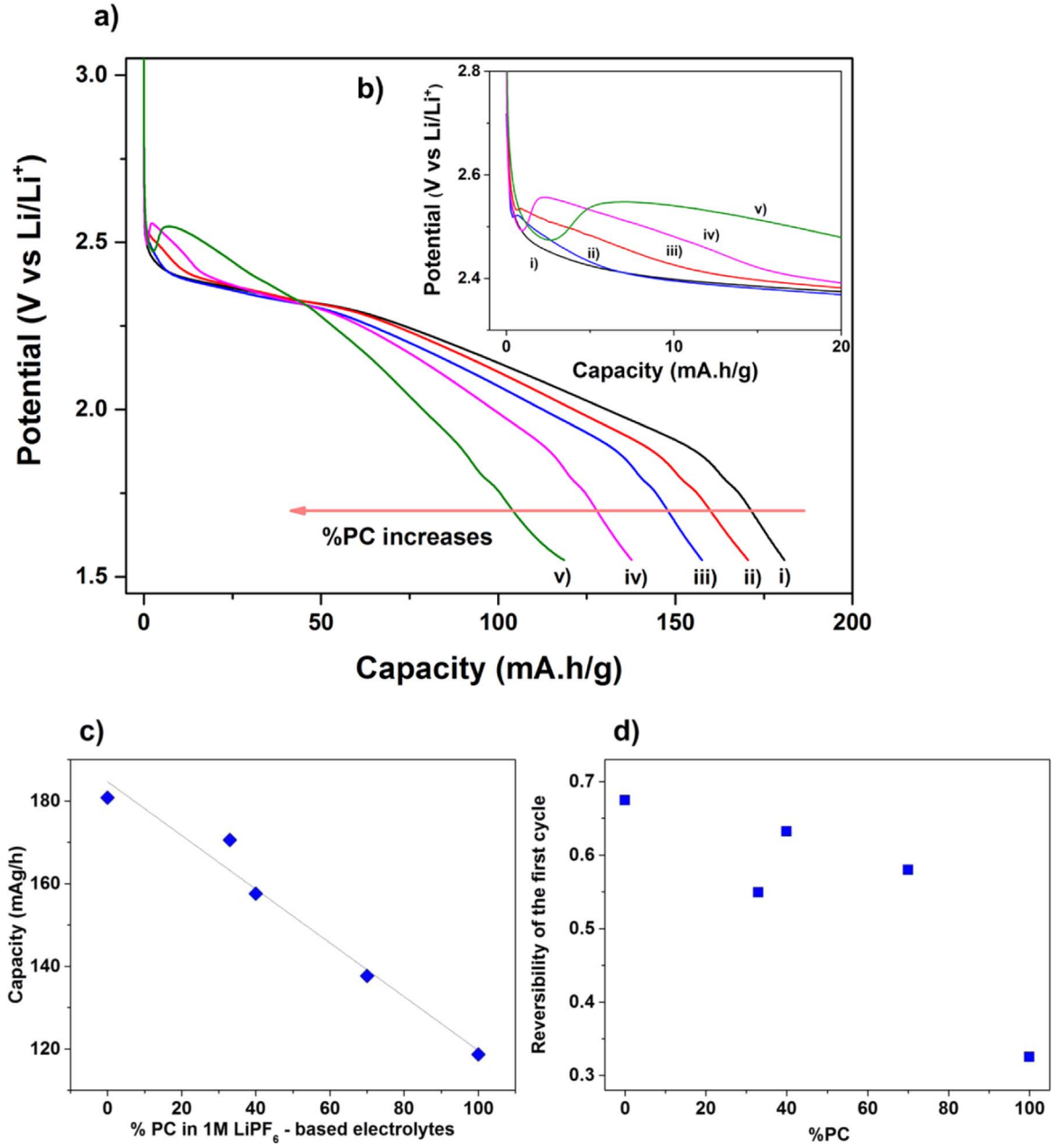

Figure 7. (a) Reduction curve at C/15 of cells cycled with 1 M $LiPF_6$ in i) EC:DMC (1:1), ii) EC:DMC:PC (33:33:33), iii) EC:DMC:PC (2:1:2), iv) EC:PC (3:7) and v) PC; (b) close-up of the early stage of discharge; (c) Resulting capacity vs the amount of PC contained in the electrolyte; (d) Reversibility of the first cycle with respect of the amount of PC contained in the electrolyte.

contains PC and the more pronounced is the bump. This feature was observed with good reproducibility in several *in situ* cells (two-electrodes) and three-electrodes Swagelok cells and coincides with the appearance of co-intercalation peaks. A similar signature was observed when inserting calcium with a $Ca(TFSI)_2$ 0,3 M in PC electrolyte.[7] Since occurring in PC containing electrolytes exclusively and at the onset of the co-intercalation phase as demonstrated by XRD experiments, it is believed this effect to reflect the nucleation of the co-intercalated phase.

Although solvent co-intercalation in TiS_2 was documented in cells using PC containing lithium,[9,24] calcium or magnesium based electrolytes,[6,7] no similar studies have been reported for sodium or potassium containing cells. The different behavior of the co-intercalated phase with respect to reversibility of its formation is most likely related to the strength of the cation interaction with the solvent. Moreover, the nature of the cation itself may also have some influence, as nicely shown by DFT studies considering the intercalation of different cations on TiS_2.[27,28]

Conclusions

The main conclusion of this study is the observation of solvent co-intercalation when reducing TiS_2 in lithium cells containing PC in the electrolyte, leading to the formation of a phase with a *c*-parameter equal to ~17.5 Å. Co-intercalation is found to be electrochemically driven and happening at the very early stages of reduction. By performing analogous experiments in different electrolytes containing different salts and with different cycling conditions (C-rate, potential window), we were able to conclude that neither the nature of the salt nor the cycling conditions have any influence in the formation of the co-intercalated phase. However, the content of PC in the electrolyte plays a major role in the amount of co-intercalated phase formed, capacity loss and

irreversibility. Co-intercalation was found to be irreversible, as this phase does not revert back to TiS_2 after reoxidation, and hence it is a source of irreversible capacity upon the first cycle. Yet, this phase does not evolve upon cycling and the formation of Li_xTiS_2 with $x = 1$ is observed in all cells. Interestingly, the formation of a co-intercalated phase was found to be reversible in Ca cells. Further investigation is needed in order to better understand the different interactions between the host structure and Li or Ca cation complexes.

Acknowledgments

The authors acknowledge funding from Ministry of Science and Innovation through grant MAT2017–86616-R, from the "Severo Ochoa" Programme for Centres of Excellence in R&D (CEX2019-000917-S). This project has received funding from the European Union's Horizon 2020 research and innovation program under the Marie Skłodowska-Curie grant agreement N° 754397. The ALBA synchrotron is acknowledged for provision of beamtime within the in-house project program (proposals 2019013225 and 2020014004).

ORCID

Raphaëlle G. Houdeville https://orcid.org/0000-0002-6100-1432
Ashley P. Black https://orcid.org/0000-0001-7929-5144
Alexandre Ponrouch https://orcid.org/0000-0002-8232-6324
M. Rosa Palacín https://orcid.org/0000-0001-7351-2005
François Fauth https://orcid.org/0000-0001-9465-3106

References

1. M. Winter, B. Barnett, and K. Xu, *Chem. Rev.*, **118**, 11433 (2018).
2. M. S. Whittingham, *Science, New Series*, **192**, 1126 (1976).
3. M. S. Whittingham, *Proc. IEEE*, **100**, 1518 (2012).
4. N. Pereira, G. G. Amatucci, M. S. Whittingham, and R. Hamlen, *J. Power Sources*, **280**, 18 (2015).
5. X. Sun, P. Bonnick, and L. F. Nazar, *ACS Energy Lett.*, **1**, 294 (2016).
6. D. S. Tchitchekova, A. Ponrouch, R. Verrelli, T. Broux, C. Frontera, A. Sorrentino, F. Bardé, N. Biskup, M. E. Arroyo-de Dompablo, and M. R. Palacín, *Chem. Mater.*, **30**, 847 (2018).
7. R. Verrelli, A. Black, R. Dugas, D. Tchitchekova, A. Ponrouch, and M. R. Palacín, *J. Electrochem. Soc.*, **167**, 070532 (2020).
8. R. R. Chianelli, J. C. Scanlon, and B. M. L. Rao, *J. Solid State Chem.*, **29**, 323 (1979).
9. J. R. Dahn, M. A. Py, and R. R. Haering, *Can. J. Phys.*, **60**, 307 (1982).
10. F. Lin et al., *Chem. Rev.*, **117**, 13123 (2017).
11. W. Rüdorff, *Chimia*, **19**, 489 (1965).
12. J. Bichon, M. Danot, and J. Rouxel, *Comptes Rendus Acad. Sci., Ser. C, Sci. Chim.*, **276**, 1283 (1973).
13. A. H. Thompson and C. R. Symon, *Solid State Ionics*, **3**, 175 (1981).
14. J. Rodriguez-Carvajal, *Physica B*, **192**, 55 (1993).
15. J. C. Panitz, U. Wietelmann, M. Wachtler, S. Ströbele, and M. Wohlfahrt-Mehrens, *J. Power Sources*, **153**, 396 (2006).
16. F. Fauth, I. Peral, C. Popescu, and M. Knapp, *Powder Diffr.*, **28**, S360 (2013).
17. F. Fauth, R. Boer, F. Gil-Ortiz, C. Popescu, O. Vallcorba, I. Peral, D. Fullà, J. Benach, and J. Juanhuix, *The European Physical Journal Plus*, **130**, 160 (2015).
18. J. B. Leriche, S. Hamelet, J. Shu, M. Morcrette, C. Masquelier, G. Ouvrard, M. Zerrouki, P. Soudan, S. Belin, and E. Elkaïm, *J. Electrochem. Soc.*, **157**, A606 (2010).
19. M. Herklotz et al., *J. Appl. Crystallogr.*, **49**, 340 (2016).
20. D. Guyomard and J. M. Tarascon, *J. Electrochem. Soc.*, **139**, 937 (1992).
21. R. Dugas, J. D. Forero-Saboya, and A. Ponrouch, *Chem. Mater.*, **31**, 8613 (2019).
22. J. Bear and F. K. McTaggart, *Aust. J. Chem.*, **11**, 458 (1958).
23. D. Saurel, J. Segalini, M. Jauregui, A. Pendashteha, B. Daffos, P. Simon, and M. Casas-Cabanas, *Energy Storage Mater.*, **21**, 162 (2019).
24. M. S. Whittingham, *Prog. Solid State Chem.*, **12**, 41 (1978).
25. J. R. Dahn, W. McKinnon, R. R. Haering, W. J. L. Buyers, and B. M. Powell, *Can. J. Phys.*, **58**, 207 (1980).
26. J. D. Forero-Saboya, E. Marchante, R. B. Araujo, D. Monti, P. Johansson, and A. Ponrouch, *The Journal of Physical Chemistry C*, **123**, 29524 (2019).
27. M. D. Radin and A. Van der Ven, *Chem. Mater.*, **28**, 7898 (2016).
28. A. Emly and A. Van der Ven, *Inorg. Chem.*, **54**, 4394 (2015).